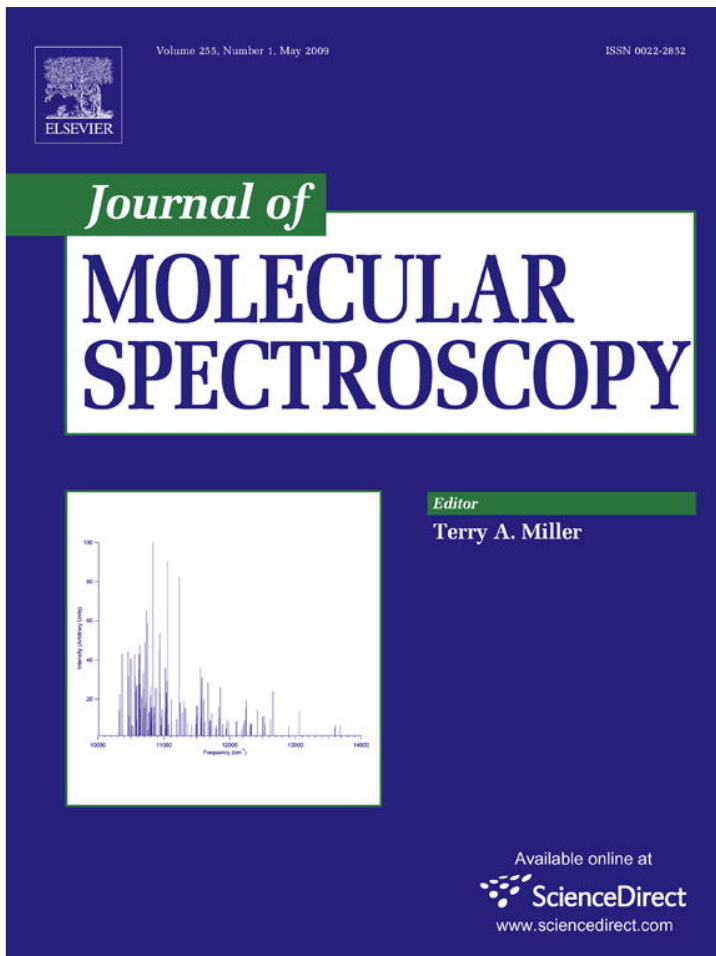


Provided for non-commercial research and education use.
Not for reproduction, distribution or commercial use.



This article appeared in a journal published by Elsevier. The attached copy is furnished to the author for internal non-commercial research and education use, including for instruction at the authors institution and sharing with colleagues.

Other uses, including reproduction and distribution, or selling or licensing copies, or posting to personal, institutional or third party websites are prohibited.

In most cases authors are permitted to post their version of the article (e.g. in Word or Tex form) to their personal website or institutional repository. Authors requiring further information regarding Elsevier's archiving and manuscript policies are encouraged to visit:

<http://www.elsevier.com/copyright>



Contents lists available at ScienceDirect

Journal of Molecular Spectroscopyjournal homepage: www.elsevier.com/locate/jms**Fourier-transform spectroscopy of $^{15}\text{N}^{14}\text{N}^{16}\text{O}$ in the 3500–9000 cm^{-1} region**

K.-F. Song, A.-W. Liu *, H.-Y. Ni, S.-M. Hu

Department of Chemical Physics, Hefei National Laboratory for Physical Sciences at Microscale, University of Science and Technology of China, JinZhai Road No. 96, Hefei 230026, China

ARTICLE INFO**Article history:**

Received 1 December 2008

In revised form 30 January 2009

Available online 21 February 2009

Keywords:

Nitrous oxide

Vibration-rotation spectroscopy

Line positions

Spectroscopic parameters

ABSTRACT

The Fourier-transform absorption spectrum of $^{15}\text{N}^{14}\text{N}^{16}\text{O}$ -enriched nitrous oxide has been recorded at the Doppler limited resolution in the spectral range 3500–9000 cm^{-1} . More than 15 000 transitions of $^{15}\text{N}^{14}\text{N}^{16}\text{O}$ were observed and assigned based on the global effective Hamiltonian model. The band-by-band analysis led to the determination of the ro-vibrational parameters of a total of 133 bands. Among these bands, 103 were newly observed, and the rotational analysis of 30 others were significantly extended and improved.

© 2009 Elsevier Inc. All rights reserved.

1. Introduction

The analysis of stable isotopes is a powerful tool for studies of the composition of the Earth's atmosphere, industrial emissions, industrial process control, ambient and workplace concentrations in view of health issues, agriculture, medical diagnostics and homeland security [1]. Today, isotope detection by laser spectroscopy, such as isotope-ratio mass spectrometry (IRMS) [2] has become an important method. In addition, infrared spectra of minor isotopologues serve as a benchmark to test the available potential energy surface (PES) and dipole moment surface (DMS). However, the high-resolution study of most minor isotopologues of many polyatomic molecules is not yet complete. Therefore, we have undertaken a systematic absorption spectroscopy study of the isotopologues of the main atmospheric species from the mid-infrared to the near-infrared: D_2^{16}O [3], H_2^{18}O [4–6], $^{13}\text{C}^{16}\text{O}_2$ [7,8], $^{12}\text{C}^{18}\text{O}_2$ [9], D^{32}S [10], and $^{14}\text{N}^{15}\text{N}^{16}\text{O}$ [11].

$^{15}\text{N}^{14}\text{N}^{16}\text{O}$ and $^{14}\text{N}^{15}\text{N}^{16}\text{O}$ are the next most abundant isotopic species of nitrous oxide after $^{14}\text{N}^{14}\text{N}^{16}\text{O}$. In the last few decades, spectroscopic studies of the $^{15}\text{N}^{14}\text{N}^{16}\text{O}$ molecule have been performed using microwave (MW) [12], Fourier-transform infrared (FTIR) [13,14], intra-cavity laser absorption spectroscopy (ICLAS) [15], and cavity ring-down spectroscopy (CRDS) [16,17]. Since most of these measurements were carried out with natural nitrous oxide samples, high resolution spectra of $^{15}\text{N}^{14}\text{N}^{16}\text{O}$ are still rather scarce, especially in the near-IR region. The present work is devoted to generating a more complete list for the line positions of the $^{15}\text{N}^{14}\text{N}^{16}\text{O}$ species in the 3500–9000 cm^{-1} region.

The present paper is organized as follows. In Section 2, the experimental conditions employed for measurement of the spectra are presented. Section 3 presents the band-by-band assignment and a summary of the ro-vibrational analysis. In Section 4, the comparisons of available results from the literature and the observed local resonance perturbations will be discussed.

2. Experimental details

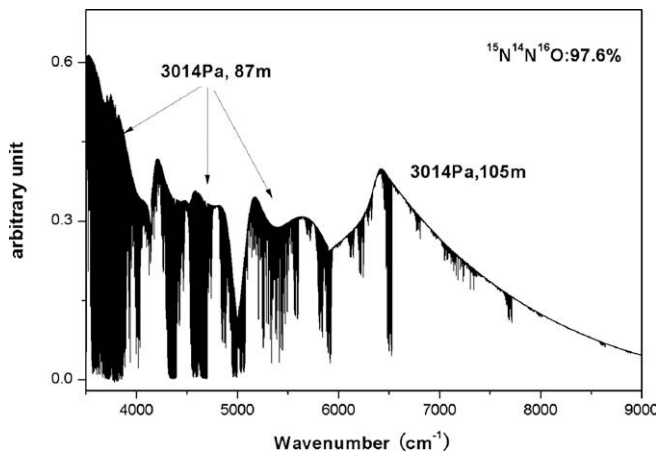
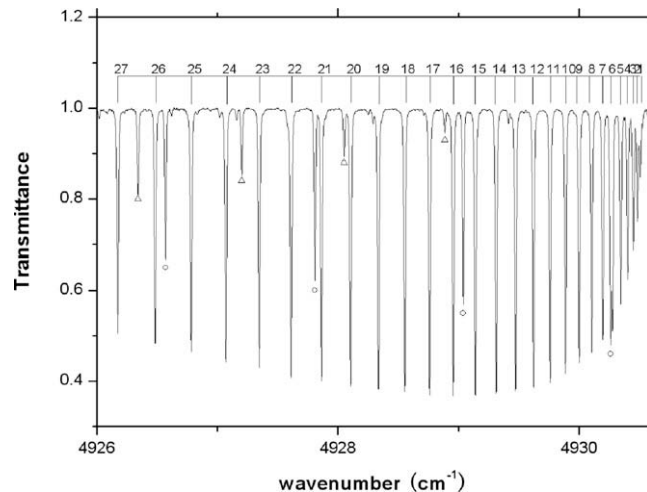
The $^{15}\text{N}^{14}\text{N}^{16}\text{O}$ -enriched nitrous oxide sample was purchased from Icon Services Inc. The stated isotope concentration is 99%. Photo-ionization mass spectroscopy (PIMS) combined with IR spectroscopy gave an abundance of 97.6% with about 0.2% uncertainty for $^{15}\text{N}^{14}\text{N}^{16}\text{O}$ in the sample. PIMS was performed with a time-of-flight mass spectrometer at the photochemistry end-station in National Synchrotron Radiation Laboratory (NSRL), Hefei. The absorption spectrum was recorded by a Bruker IFS 120HR interferometer with a path length adjustable multi-pass gas cell. The interference chamber was evacuated to 0.4 mbar to eliminate atmospheric absorption. Because of the wide spectral range and the large variations in absorption band intensities, different experimental conditions were applied for the measurements, as listed in Table 1. The gas sample pressure was measured using two capacitance manometers (MKS Baratron 627B) with 1 and 20 Torr full-scale ranges and an accuracy of 0.15%. In most measurements, different optical filters were applied to improve the signal-to-noise ratio and to allow for high-resolution measurements. The lines for water and carbon dioxide in the interference chamber were used to calibrate the spectra. Their values were taken from the HITRAN2004 database [18]. The accuracies of the unblended and not-very-weak lines are estimated to be better than 0.001 cm^{-1} . An overview of the recorded spectrum is presented in Fig. 1.

* Corresponding author. Fax: +86 551 3602969.

E-mail address: awliu@mail.ustc.edu.cn (A.-W. Liu).

Table 1Experimental conditions of FTIR spectra of $^{15}\text{N}^{14}\text{N}^{16}\text{O}$ -enriched nitrous oxide sample.

Range (cm^{-1})	Pressure (Pa)	Detector	Path length (m)	Resolution (cm^{-1})	Temperature (K)
5000–9000	3014	Ge	105	0.015	298
5000–9000	3014	Ge	87	0.015	297
5000–9000	3014	Ge	51	0.015	299
5000–9000	3014	Ge	15	0.015	298
5000–9000	1014	Ge	51	0.015	300
5000–9000	1014	Ge	15	0.015	300
5000–6300	3014	InSb	105	0.013	298
5000–6300	3014	InSb	87	0.010	297
5000–6300	3014	InSb	15	0.010	298
5000–6300	1014	InSb	15	0.008	300
4100–5000	3014	InSb	87	0.010	297
4100–5000	3014	InSb	15	0.008	299
4100–5000	1014	InSb	15	0.008	301
4100–5000	235	InSb	15	0.008	299
3300–4300	3014	InSb	87	0.010	298
3300–4300	3014	InSb	15	0.008	300
3300–4300	1014	InSb	15	0.008	300
3300–4300	235	InSb	15	0.008	299
3300–4300	56	InSb	15	0.008	297

**Fig. 1.** Overview of the Fourier-transform absorption spectrum of $^{15}\text{N}^{14}\text{N}^{16}\text{O}$ in the 3500–9000 cm^{-1} region.**Fig. 2.** The Q-branch of the 0112f-0000e $\Pi-\Sigma$ cold band of $^{15}\text{N}^{14}\text{N}^{16}\text{O}$ at 4930.52 cm^{-1} and the rotational assignments are presented. The spectrum was recorded at a pressure of 3014 Pa and an equivalent absorption path length of 87 m. The lines marked by open circles and open triangles correspond to the 4000e-0000e and the 0112e-0000e band transitions of $^{15}\text{N}^{14}\text{N}^{16}\text{O}$ centered at 4976.65 and 4930.52 cm^{-1} , respectively.

3. Ro-vibrational analysis

3.1. Vibrational assignment

The observed transitions were assigned based on the predictions of the effective ro-vibration Hamiltonian developed by Teffo et al. [19]. The preliminary set of the effective Hamiltonian parameters for $^{15}\text{N}^{14}\text{N}^{16}\text{O}$ was derived by Vlasova et al. [20].

A total of 133 vibrational bands were assigned for $^{15}\text{N}^{14}\text{N}^{16}\text{O}$ in the studied region. Except for the eight $\Pi-\Sigma$ and six $\Delta-\Sigma$ cold bands and the one $\Pi-\Sigma$, four $\Sigma-\Pi$, four $\Delta-\Pi$ and one $\Phi-\Delta$ hot bands, all other analyzed bands were parallel bands ($\Delta l_2 = 0$): 37 $\Sigma-\Sigma$ cold bands, 34 $\Sigma-\Sigma$ hot bands, 24 $\Pi-\Pi$ bands, and 14 $\Delta-\Delta$ bands. For illustration, Fig. 2 presents the Q branch head of the perpendicular cold band 0112f-0000e (normal mode notation: $V_1V_2\ell_2V_3$) centered at 4930.52 cm^{-1} . As another example, the R-branch of the parallel hot band 1113-0110 is shown in Fig. 3, as well as the P-branch of the 1003e-0000e band.

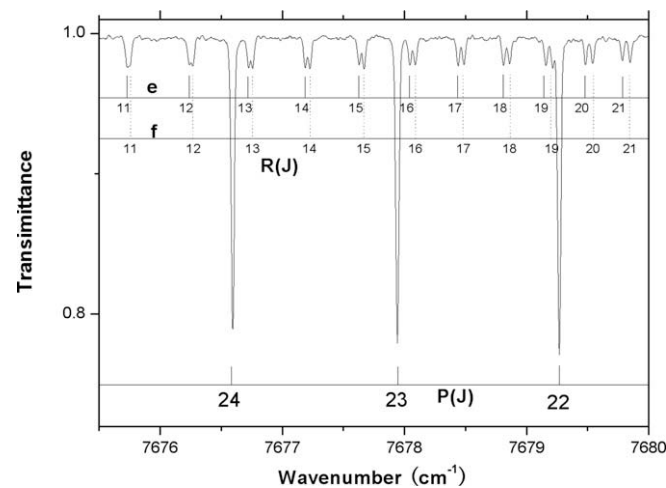
**Fig. 3.** The P-branch of the 1003e-0000e $\Sigma-\Sigma$ cold band of $^{15}\text{N}^{14}\text{N}^{16}\text{O}$ at 7702.50 cm^{-1} and the R-branch of the 1113-0110 $\Pi-\Pi$ hot band of $^{15}\text{N}^{14}\text{N}^{16}\text{O}$ at 7667.81 cm^{-1} . The spectrum was recorded at a pressure of 3014 Pa and an equivalent absorption path length of 105 m. The rotational assignments are also presented.

Table 2Spectroscopic parameters (in cm^{-1}) of the vibrational bands of $^{15}\text{N}^{14}\text{N}^{16}\text{O}$ assigned in the 3500–9000 cm^{-1} region.

Lower states constants [22]		G_v	B_v	$D_v \times 10^7$		$H_v \times 10^{12}$			
$V_1V_2V_3l_2V_3$				(cm^{-1})	(cm^{-1})				
0000e		0.0		0.404857965		1.642938			
0110e		585.31212		0.405037265		1.656798			
0110f		585.31212		0.405781109		1.667421			
0200e		1159.97171		0.405712750		2.227530			
0220e		1170.84300		0.405951200		1.218000			
ΔG_v^{a} (cm^{-1})	Type	Bands ^b	G_v (cm^{-1})	B_v (cm^{-1})	$D_v \times 10^7$ (cm^{-1})	$H_v \times 10^{12}$ (cm^{-1})			
						Observed lines			
						n/N^{c}			
						RMS $\times 10^3$			
						In Refs. ^d			
<i>Cold bands</i>									
3589.92766(19)	$\Sigma-\Sigma$	2200e–0000e	3589.92766(19)	0.40464974(47)	3.2343(27)	7.994(39)	P70/R68	122/135	0.97
3589.9301(1)		1400e–0000e ^A		0.4046484(5)	3.199(8)	6.4(3)	P42/R39	/72	0.25
		1400e–0000e ^T	3589.9283(11)	0.4046458(12)	3.1904(62)	6.4(12)			
3602.0376(16)	$\Delta-\Sigma$	2220e–0000e	3602.0376(16)	0.4049350(34)	0.553(21)	−8.77(39)	P55/R57	40/58	1.00
3712.12845(14)	$\Sigma-\Sigma$	3000e–0000e	3712.12845(14)	0.40233347(30)	2.1490(15)	1.705(19)	P76/R72	134/142	0.73
3712.1310(1)		2200e–0000e ^A		0.4023350(1)	2.157(1)	1.87(3)	P50/R51	/89	0.11
		2200e–0000e ^T	3712.12854(17)	0.40233302(54)	2.148563(89)	1.7688(96)			
3733.80519(99)	$\Delta-\Sigma$	2220e–0000e	3733.80519(99)	0.4032340(24)	1.236(15)	−2.10(28)	P57/R58	40/56	0.94
3795.45068(11)	$\Sigma-\Sigma$	3000e–0000e	3795.45068(11)	0.40064203(30)	1.2400(18)	2.076(28)	P68/R67	123/132	0.58
3795.4535(1)		3000e–0000e ^A		0.4006431(2)	1.242(2)	2.06(4)	P27/R54	/89	0.24
		3000e–0000e ^T	3795.45089(21)	0.40064084(28)	1.2292(43)	1.78(14)			
3896.77599(32)	$\Pi-\Sigma$	0311e–0000e	3896.77599(32)	0.4021712(11)	1.9101(67)		P42/R41	62/75	1.24
3896.77614(43)		0311f–0000e	3896.77614(43)	0.4035324(12)	1.9955(62)		Q45	29/38	1.00
4022.28962(21)	$\Pi-\Sigma$	1111f–0000e	4022.28962(21)	0.40100740(59)	1.5626(31)		Q47	44/47	0.69
4022.2913(1)		1111f–0000e ^A		0.401008(1)	1.713(10)		Q65	/63	0.1
4022.28977(19)		1111e–0000e	4022.28977(19)	0.40016322(76)	1.6092(70)	0.56(17)	P58/R56	102/113	0.81
4022.2913(1)		1111e–0000e ^A		0.4001642(2)	1.600(2)		P39/R36	/70	0.23
4162.69408(23)	$\Pi-\Sigma$	0710e–0000e	4162.69408(23)	0.4038873(12)	2.352(16)	4.17(57)	P31/R44	60/68	0.72
4162.69493(20)		0710f–0000e	4162.69493(20)	0.40602970(51)	2.4506(24)		Q47	43/46	0.63
4296.71797(24)	$\Pi-\Sigma$	3110e–0000e	4296.71797(24)	0.4020302(11)	1.910(13)	1.44(40)	P34/R48	59/71	0.80
4296.71800(33)		3110f–0000e	4296.71800(33)	0.4036713(10)	1.9172(57)		Q43	28/33	0.88
4373.60576(9)	$\Sigma-\Sigma$	0002e–0000e	4373.60576(9)	0.39813063(18)	1.6341(9)	0.185(11)	P81/R80	142/155	0.48
4373.6093(1)		0002e–0000e ^A		0.3981321(3)	1.642(2)	0.28(4)	P59/R55	/60	0.37
		0002e–0000e ^T	4373.60609(8)	0.398130258(72)	1.63054(73)				
4404.83873(16)	$\Pi-\Sigma$	2310f–0000e	4404.83873(16)	0.40210290(40)	1.1840(18)		Q49	42/46	0.51
4404.83848(22)		2310e–0000e	4404.83848(22)	0.40079442(90)	1.4175(88)	0.93(22)	P38/R51	53/66	0.65
4452.11685(6)	$\Sigma-\Sigma$	0401e–0000e	4452.11685(60)	0.40314542(20)	3.3827(14)	10.186(25)	P58/R64	116/120	0.32
4452.1189(2)		0401e–0000e ^A		0.4031409(10)	3.227(10)		P27/R31	/43	0.49
4461.1986(14)	$\Delta-\Sigma$	0421e–0000e	4461.1986(14)	0.4033327(32)	0.541(21)	−8.58(41)	P52/R54	44/52	0.99
4585.66912(15)	$\Sigma-\Sigma$	1201e–0000e ^e	4585.66912(15)	0.40076476(51)	2.2067(40)	2.925(84)	P70/R67	103/136	0.70
4585.671(1)		1201e–0000e ^A		0.400768(3)	2.239(30)	3.6(6)	P49/R56	/105	5.3
4585.67001		1201e–0000e ^T	4585.67001(60)	0.4007635(13)	2.225(23)	5.10(12)			
4600.05189(56)	$\Delta-\Sigma$	1221e–0000e	4600.05189(56)	0.4012330(13)	1.2079(88)	−2.04(17)	P58/R56	68/74	0.84
4679.91810(7)	$\Sigma-\Sigma$	2001e–0000e	4679.91810(7)	0.39841914(15)	1.4737(8)	1.040(12)	P74/R65	130/136	0.35
4679.9216(1)		2001e–0000e ^A		0.3984210(4)	1.483(3)	1.13(6)	P60/R50	/73	0.48
4679.91818		2001e–0000e ^T	4679.91818(4)	0.39841777(14)	1.46279(39)	0.9647(61)			
4726.84465(11)	$\Sigma-\Sigma$	0800e–0000e	4726.84465(11)	0.40511099(52)	4.9456(53)	24.18(14)	P49/R55	81/91	0.46
4737.33630(47)	$\Delta-\Sigma$	0820e–0000e	4737.33630(47)	0.4054461(68)	0.358(24)		P36/R45	15/19	0.88
4866.89056(9)	$\Sigma-\Sigma$	3200e–0000e	4866.89056(9)	0.40287032(24)	3.0831(15)	6.529(26)	P66/R65	132/132	0.45
4866.8926(1)		2400e–0000e ^A		0.4028713(6)	3.087(13)	6.8(7)	P29/R35	/58	0.38
4882.7978(16)	$\Delta-\Sigma$	3220e–0000e	4882.7978(16)	0.4033904(36)	0.791(24)	−5.72(47)	P58/R48	39/49	0.83
4930.51795(11)	$\Pi-\Sigma$	0112e–0000e	4930.51795(11)	0.39839594(35)	1.6635(26)	0.438(49)	P61/R60	104/110	0.50
4930.51809(6)		0112f–0000e	4930.51809(6)	0.39911120(10)	1.6648(3)		Q62	59/61	0.27
4930.520(1)		0112f–0000e ^A		0.3991116(40)	1.630(30)		Q31	/24	0.18
4976.64895(7)	$\Sigma-\Sigma$	4000e–0000e	4976.64895(7)	0.40049305(18)	2.0879(11)	2.533(17)	P69/R67	131/133	0.36
4976.6513(1)		3200e–0000e ^A		0.4004938(2)	2.086(2)	2.45(7)	P45/R47	/92	0.17
4976.64973		3200e–0000e ^T	4976.64973(40)	0.40048913(83)	2.0212(50)				
5054.90845(11)	$\Sigma-\Sigma$	3200e–0000e	5054.90845(11)	0.39986761(36)	0.8332(28)	3.514(56)	P61/R59	118/122	0.52
5054.9112(1)		4000e–0000e ^A		0.3998676(4)	0.815(6)	2.6(2)	P42/R43	/83	0.46
5054.90941		4000e–0000e ^T	5054.90941(67)	0.39986471(61)	0.7695(66)				
5266.71571(38)	$\Pi-\Sigma$	2111e–0000e	5266.71571(38)	0.3987381(17)	1.510(13)		P27/R33	49/66	1.21
5266.71576(28)		2111e–0000e	5266.71576(28)	0.3997545(10)	1.4245(72)		Q41	28/38	0.67
5477.91870(12)	$\Sigma-\Sigma$	0202e–0000e	5477.91870(12)	0.39913180(56)	2.2291(63)	2.36(18)	P52/R51	85/98	0.47
5587.86194(06)	$\Sigma-\Sigma$	1002e–0000e	5587.86194(06)	0.39649681(20)	1.5810(15)	0.322(28)	P63/R60	110/121	0.30
5709.25072(8)	$\Sigma-\Sigma$	2201e–0000e ^e	5709.25072(8)	0.40142636(41)	3.2244(47)	9.33(15)	P56/R55	93/111	0.34
5829.91013(7)	$\Sigma-\Sigma$	3001e–0000e	5829.91013(7)	0.39901752(21)	2.1417(14)	1.608(25)	P65/R64	123/130	0.35
5829.9097(4)		2201e–0000e ^A	5829.9097(4)	0.3990266(38)	2.305(81)	1.05(46)	P33/R35	/58	0.68
5852.9884(14)	$\Sigma-\Sigma$	3400e–0000e	5852.9884(14)	0.4054579(69)	6.677(76)		P25/R28	22/28	1.59
5911.94747(7)	$\Sigma-\Sigma$	3001e–0000e	5911.94747(7)	0.39724916(25)	1.1996(19)	2.251(37)	P61/R55	112/117	0.36
5911.9482(2)		3001e–0000e ^A	5911.9482(2)	0.3972481(08)	1.156(07)		P26/R33	/44	0.96
5911.94814		3001e–0000e ^T	5911.94814(24)	0.3972420(77)	1.06(12)				
5911.94525(26)		3001e–0000e ^{L2}	5911.94525(26)	0.3972470(11)	1.175(10)	1.39(24)	P7/R55	44/50	0.9
6005.8570(22)	$\Sigma-\Sigma$	4200e–0000e	6005.85699(22)	0.4032609(14)	4.680(21)	20.09(80)	P42/R41	78/84	0.78
6005.85785(80)		4200e–0000e ^{L2}	6005.85785(80)	0.4032562(41)	4.644(54)		R41	30/30	1.1
6135.36485(11)	$\Sigma-\Sigma$	5000e–0000e	6135.36485(11)	0.40096497(43)	2.9362(38)	5.186(86)	P57/R58	109/116	0.52

Table 2 (continued)

ΔG_v^a (cm $^{-1}$)	Type	Bands ^b	G_v (cm $^{-1}$)	B_v (cm $^{-1}$)	$D_v \times 10^7$ (cm $^{-1}$)	$H_v \times 10^{12}$ (cm $^{-1}$)	Observed lines	n/N ^c	RMS $\times 10^3$	In Refs. ^d
6135.36629(32)		5000e–0000e ^{l2}	6135.36629(32)	0.4009582(11)	2.8282(75)		P45/R34	58/65	1.1	
6152.40423(63)	$\Pi-\Sigma$	1112e–0000e	6152.40423(63)	0.3968420(33)	1.697(32)		P34/R25	27/45	1.28	
6152.40624(55)		1112f–0000e	6152.40624(55)	0.3976544(23)	1.576(19)		Q35	25/31	1.23	
6232.91517(6)	$\Sigma-\Sigma$	5000e–0000e	6232.91517(6)	0.39873059(19)	1.7577(13)	4.579(25)	P59/R62	108/120	0.30	
6232.91734(34)		5000e–0000e ^{l1}	6232.91734(34)	0.39871840(87)	1.6093(38)		P49/R49	83/89	1.7	
6315.01438(8)	$\Sigma-\Sigma$	3400e–0000e	6315.01438(8)	0.39942374(33)	0.3678(34)	5.809(91)	P55/R53	98/107	0.34	
6315.01651(38)		3400e–0000e ^{l1}	6315.01651(38)	0.3994122(11)	0.2073(54)		P46/R46	59/64	1.4	
6515.98628(10)	$\Sigma-\Sigma$	0003e–0000e ^e	6515.98628(10)	0.39476260(43)	1.6528(42)	1.05(11)	P69/R59	91/122	0.46	
6515.98762(20)		0003e–0000e ^{l1}	6515.98762(20)	0.39475860(42)	1.6185(16)		P58/R45	77/85	1.0	
6569.54894(38)	$\Sigma-\Sigma$	0402e–0000e	6569.54894(38)	0.3999293(32)	3.566(62)	21.4(32)	P35/R37	60/68	1.16	
6702.35199(13)	$\Sigma-\Sigma$	1202e–0000e	6702.35199(13)	0.39745218(74)	2.1447(98)	1.38(34)	P48/R58	89/107	0.53	
6702.35285(31)		0402e–0000e ^{l1}	6702.35285(31)	0.3944770(88)	2.0975(47)		P37/R46	71/76	1.4	
6795.93245(9)	$\Sigma-\Sigma$	2002e–0000e	6795.93245(9)	0.39501766(41)	1.4469(42)	0.78(11)	P52/R52	96/104	0.41	
6795.93260(26)		2002e–0000e ^{l1}	6795.93260(26)	0.39501620(57)	1.4269(23)		P52/R50	79/80	1.2	
6957.90065(20)	$\Sigma-\Sigma$	3201e–0000e	6957.90065(20)	0.3996444(11)	3.079(13)	7.31(43)	P45/R47	80/93	0.76	
7065.52508(11)	$\Sigma-\Sigma$	4001e–0000e	7065.52508(11)	0.39714574(49)	2.0935(49)	2.79(13)	P53/R52	97/106	0.49	
7142.12893(10)	$\Sigma-\Sigma$	3201e–0000e ^e	7142.12893(10)	0.39653682(83)	0.817(16)	12.60(86)	P48/R46	71/92	0.34	
7394.27264(31)	$\Sigma-\Sigma$	6000e–0000e	7394.27264(31)	0.3988685(11)	2.6692(71)		P35/R42	57/76	1.15	
7482.85694(31)	$\Sigma-\Sigma$	6000e–0000e	7482.85694(31)	0.3974403(11)	0.8931(64)		P38/R42	62/80	1.31	
7592.48600(36)	$\Sigma-\Sigma$	0203e–0000e	7592.48600(36)	0.3958415(12)	2.1972(77)		P48/R45	69/92	1.55	
7702.50017(18)	$\Sigma-\Sigma$	1003e–0000e	7702.50017(18)	0.39310735(42)	1.5688(17)		P55/R53	88/105	0.93	
7918.58511(52)	$\Sigma-\Sigma$	3002e–0000e	7918.58511(52)	0.3957961(37)	3.139(63)	34.5(29)	P39/R40	62/77	1.43	
7999.43103(26)	$\Sigma-\Sigma$	3002e–0000e	7999.43103(26)	0.3938620(11)	1.1565(78)		P40/R36	61/77	0.99	
8292.13033(66)	$\Sigma-\Sigma$	5001e–0000e	8292.13033(66)	0.3953424(34)	1.413(36)		P28/R31	34/50	1.48	
8628.68498(29)	$\Sigma-\Sigma$	0004e–0000e	8628.68498(29)	0.3914153(18)	1.743(28)	3.4(11)	P44/R31	62/75	1.00	
8882.51591(57)	$\Sigma-\Sigma$	2003e–0000e	8882.51591(57)	0.3916341(41)	1.702(68)	18.7(31)	P40/R37	55/69	1.52	
<i>Hot bands</i>										
3519.94700(25)	$\Sigma-\Sigma$	2001e–0200e	4679.91871(25)	0.39841442(90)	1.4377(58)		P41/R41	55/73	0.95	2001e–0000e ^A
3566.54183(45)	$\Delta-\Delta$	0820e–0220e	4737.38483(45)	0.4053304(31)	-0.468(49)	-15.0(21)	P43/R39	47/71	1.28	
3566.54261(50)		0820f–0220f	4737.38561(50)	0.4053409(41)	2.589(71)	12.6(33)	P43/R39	45/73	1.33	
3566.87323(59)	$\Sigma-\Sigma$	0800e–0200e	4726.84494(59)	0.4051100(29)	4.963(38)	25.2(14)	P45/R44	51/72	1.16	
3577.38225(28)	$\Pi-\Pi$	2310f–0110f	4162.69437(28)	0.4060311(11)	2.456(10)	0.15(25)	P55/R59	83/105	1.07	
3577.38311(25)		2310e–0110e	4162.69523(25)	0.40388197(96)	2.2906(86)	2.19(20)	P60/R52	86/106	0.97	
3596.99781(55)	$\Sigma-\Sigma$	3200e–1000e	4866.88979(55)	0.4028758(41)	3.208(78)	14.4(40)	P39/R37	36/63	1.04	2400e–0000e ^A
3706.75727(27)	$\Sigma-\Sigma$	4000e–1000e	4976.64925(27)	0.4004926(13)	2.086(14)	2.49(38)	P52/R48	90/73	1.05	3200e–0000e ^A
3706.91871(35)	$\Sigma-\Sigma$	3200e–0200e	4866.89042(35)	0.4028734(18)	3.140(22)	8.76(66)	P49/R47	63/80	1.29	2400e–0000e ^A
3711.40604(15)	$\Pi-\Pi$	3110f–0110f	4296.71816(15)	0.40367160(52)	1.9242(41)	0.408(87)	P64/R63	105/119	0.65	
3711.4084(1)		2310f–0110f ^a		0.4036737(6)	1.966(14)	3.1(9)	P33/R29	/53	0.16	
3711.40762		2310f–0110f ^r	4296.71794(74)	0.4036763(55)	2.09(19)	11(13)				
3711.40605(15)		3110e–0110e	4296.71817(15)	0.40202836(43)	1.8872(28)	0.779(48)	P66/R64	99/113	0.66	
3711.4084(1)		2310e–0110e ^A		0.4020286(5)	1.871(5)		P32/R30	/42	0.25	
3711.40291		2310e–0110e ^r	4296.71503(23)	0.4020705(14)	3.03(36)	79(23)				
3711.40656(88)		3110e–0110f	4296.71868(88)	0.4020692(85)	2.92(15)		Q23	8/13	0.99	
3711.408(35)		3110f–0110e	4296.720(35)	0.40366(37)	2.0(91)		Q16	4/6	3.70	
3711.95153(87)	$\Delta-\Delta$	3220f–0220e	4882.79453(87)	0.403455(30)	3.0(21)		Q11	7/10	0.82	
3711.95609(47)		3220f–0220f	4882.79909(47)	0.4033933(34)	1.993(51)	4.5(20)	P42/R43	48/75	1.33	
3711.95722(39)		3220e–0220e	4882.80022(39)	0.4033631(36)	0.306(70)	-26.1(36)	P41/R37	42/64	0.99	
3785.01649(28)	$\Sigma-\Sigma$	3200e–1000e	5054.90847(28)	0.3998677(15)	0.834(18)	3.64(55)	P46/R46	67/80	0.94	4000e–0000e ^A
3816.67698(39)	$\Sigma-\Sigma$	4000e–0200e	4976.64869(39)	0.4004953(24)	2.132(35)	4.2(14)	P46/R44	53/70	1.08	3200e–0000e ^A
3819.52317(67)	$\Pi-\Pi$	2310e–0110f	4404.83529(67)	0.4008445(81)	2.52(19)		Q23	8/14	0.67	
3819.52678(10)		2310e–0110e	4404.83890(10)	0.40079319(31)	1.4073(21)	0.705(38)	P61/R62	101/117	0.45	
3819.5288(1)		3110e–0110e ^A		0.4007958(5)	1.426(10)	1.1(5)	P32/R35	/53	0.17	
3819.52577		3110e–0110e ^r	4404.83789(45)	0.4007953(22)	1.331(65)	-8.6(40)				
3819.52681(13)		2310f–0110f	4404.83893(13)	0.40210337(39)	1.1935(26)	0.748(46)	P65/R61	95/112	0.58	
3819.5288(1)		3110f–0110f ^a		0.4021060(5)	1.232(12)	2.5(6)	P24/R34	/45	0.17	
3819.52792		3110f–0110f ^r	4404.84004(86)	0.4020891(25)	0.877(58)	-17.5(28)				
3819.5296(21)		2310f–0110e	4404.8417(21)	0.402023(33)	-1.3(10)		Q19	7/13	1.19	
3838.31529(71)	$\Delta-\Delta$	2420f–0220e	5009.15829(71)	0.4020974(78)	1.46(17)		Q22	9/13	1.04	
3838.31595(44)		2420e–0220e	5009.15895(44)	0.4020962(30)	1.471(44)	5.1(17)	P44/R41	47/66	1.23	
3838.31679(45)		2420f–0220f	5009.15979(45)	0.4020717(31)	1.139(44)	-7.9(17)	P41/R42	48/67	1.25	
3894.93613(39)	$\Sigma-\Sigma$	3200e–0200e	5054.90784(39)	0.3998684(25)	0.842(38)	4.3(15)	P40/R44	49/73	1.07	4000e–0000e ^A
4000.35786(35)	$\Sigma-\Pi$	1201e–0110e	4585.66998(35)	0.4007587(11)	2.1149(69)		P42/R40	51/74	1.02	1201e–0000e ^A
4000.35966(45)		1201e–0110f	4585.67178(45)	0.4007563(14)	2.1133(84)		Q44	28/41	1.04	
4014.74002(38)	$\Delta-\Pi$	1221e–0110e	4600.05214(38)	0.4012348(14)	1.2470(96)		P40/R37	59/70	1.34	1220e–0220e ^A
4014.73976(41)		1221f–0110f	4600.05188(41)	0.4012336(14)	1.5983(90)		P41/R39	57/71	1.37	
4014.73971(38)		1221f–0110e	4600.05183(38)	0.4012324(12)	1.5781(74)		Q45	24/43	0.82	
4014.73887(55)		1221e–0110f	4600.05099(55)	0.4012377(11)	1.2745(46)		Q49	24/42	0.99	
4094.60657(33)	$\Sigma-\Pi$	2001e–0110e	4679.91869(33)	0.3984168(11)	1.4431(73)		P42/R36	59/72	1.17	2001e–0000e ^A
4094.60722(32)		2001e–0110f	4679.91934(32)	0.39841240(92)	1.4198(45)		Q47	36/46	1.06	
4208.02547(46)	$\Sigma-\Sigma$	0202e–1000e	5477.91745(46)	0.3991310(22)	2.206(22)		P30/R31	37/43	1.05	0202e–0200e ^A
4297.49297(76)	$\Delta-\Pi$	3220e–0110e					P10/R6	0/10		
4317.01014(24)	$\Delta-\Delta$	0222f–0220f	5487.85314(24)	0.3993704(94)	1.7018(73)	0.29(15)	P58/R55	80/106	0.98	
4317.01060(36)		0222f–0220e	5487.85360(36)	0.3993588(82)	0.67(34)		Q21	11/16	0.56	
4317.01157(35)		0222e–0220e	5487.85457(35)	0.3993606(14)	1.155(12)	-0.70(26)	P57/R55	69/101	1.38	

(continued on next page)

Table 2 (continued)

ΔG_v^a (cm $^{-1}$)	Type	Bands ^b	G_v (cm $^{-1}$)	B_v (cm $^{-1}$)	$D_v \times 10^7$ (cm $^{-1}$)	$H_v \times 10^{12}$ (cm $^{-1}$)	Observed lines	n/N^c	RMS $\times 10^3$	In Refs. ^d
4317.94620(15)	$\Sigma-\Sigma$	0202e–0200e	5477.91791(15)	0.39913220(47)	2.2334(33)	2.510(62)	P64/R54	97/108	0.65	
4317.0127(2)		0202e–0200e ^A		0.399365(4)	1.420(31)		P30/R30	/40	0.35	
4317.96910(10)	$\Sigma-\Sigma$	1002e–1000e	5587.86108(10)	0.39649653(39)	1.5772(35)	0.203(85)	P54/R52	82/94	0.37	
4345.20563(18)	$\Pi-\Pi$	0112f–0110f	4930.51775(18)	0.39911046(37)	1.6580(18)	-0.022(25)	P72/R71	106/130	0.65	
4345.2080(1)		0112f–0110f ^A		0.3991109(1)	1.6586(7)		P47/R41	/70	0.18	
4345.20570(62)		0112f–0110e	4930.51782(62)	0.3991073(40)	1.623(48)		Q30	20/22	1.43	
4345.20591(12)		0112e–0110e	4930.51803(12)	0.39839400(16)	1.6454(4)		P69/R69	98/131	0.54	
4345.2080(1)		0112e–0110e ^A		0.3983950(1)	1.6507(6)		P47/R42	/72	0.15	
4345.20641(46)		0112e–0110f	4930.51853(46)	0.3983816(54)	1.36(11)		Q25	16/20	0.95	
4397.80520(61)	$\Delta-\Delta$	0621e–0220e	5568.64820(61)	0.4039208(22)	-0.271(16)		P32/R36	23/36	1.18	
4397.80901(55)		0621f–0220f	5568.65201(55)	0.4039037(22)	2.471(18)		P32/R35	28/36	1.18	
4423.84705(66)	$\Delta-\Pi$	2420f–0110f	5009.15917(66)	0.4020871(21)	1.345(14)		R37	20/24	0.91	
4423.85048(67)		2420e–0110e	5009.16260(67)	0.4020783(20)	1.311(12)		R40	19/25	0.96	
4424.23873(12)	$\Pi-\Pi$	0511e–0110e	5009.55085(12)	0.40252113(50)	2.3678(48)	4.05(12)	P51/R52	82/91	0.45	
4424.23907(12)		0511f–0110f	5009.55119(12)	0.40448425(60)	2.4797(67)	-0.66(20)	P48/R52	76/90	0.43	
4427.88938(35)	$\Sigma-\Sigma$	1002e–0200e	5587.86109(35)	0.3964973(13)	1.5757(92)		P40/R44	57/72	1.33	
4469.5968(13)	$\Sigma-\Pi$	3200e–0110e	5054.9090(13)	0.3998619(38)	0.737(24)		P27/R38	19/23	1.50	4000e–0000e ^A
4469.5977(18)		3200e–0110f	5054.9098(18)	0.399858(14)	0.64(23)		Q22	10/17	1.05	
4549.27811(14)	$\Sigma-\Sigma$	2201e–0200e	5709.24982(14)	0.40142605(75)	3.2179(93)	9.11(30)	P51/R49	90/97	0.58	
4550.05772(21)	$\Delta-\Delta$	2221e–0220e	5720.90072(21)	0.40172522(95)	0.601(11)	-6.45(31)	P53/R46	63/85	0.70	
4550.05839(26)		2221f–0220e	5720.90139(26)	0.401711(12)	-0.5(10)		Q14	8/12	0.30	
4550.05842(23)		2221f–0220f	5720.90142(23)	0.40172943(97)	1.9837(99)	1.91(27)	P52/R51	70/89	0.79	
4560.01706(12)	$\Sigma-\Sigma$	3001e–1000e	5829.90904(12)	0.39901948(58)	2.1673(67)	2.50(21)	P49/R47	76/89	0.44	2201e–0000e ^A
4567.21812(14)	$\Pi-\Pi$	2111f–0110f	5152.53024(14)	0.40195240(47)	2.0147(37)	1.389(80)	P62/R60	91/116	0.57	
4567.2212(2)		1311f–0110f ^A		0.4019490(6)	1.9665(4)		P37/R38	/60	0.55	
4567.21829(34)		2111f–0110e	5152.53041(34)	0.4019558(57)	2.16(18)		Q18	8/15	0.41	
4567.21891(10)		2111e–0110e	5152.53103(10)	0.40048326(27)	1.9119(17)	0.963(29)	P65/R62	106/122	0.40	
4567.2212(2)		1311e–0110e ^A		0.4004838(8)	1.892(7)		P31/R34	/53	0.6	
4567.22011(31)		2111e–0110f	5152.53223(31)	0.4004693(59)	1.43(23)		Q15	8/13	0.30	
4642.05510(11)	$\Sigma-\Sigma$	3001e–1000e	5911.94708(11)	0.39724771(46)	1.1850(44)	1.85(11)	P55/R52	87/97	0.45	3001e–0000e ^A
4669.93774(14)	$\Sigma-\Sigma$	3001e–0200e	5829.90945(14)	0.39901672(80)	2.132(10)	1.27(35)	P47/R44	73/80	0.55	2201e–0000e ^A
4680.06742(19)	$\Delta-\Delta$	2221e–0220e	5850.91042(19)	0.39995665(95)	1.287(10)	1.96(28)	P52/R50	66/79	0.72	
4680.06770(9)		2221f–0220e	5850.91070(9)	0.3999459(24)	1.08(11)		Q14	8/10	0.12	
4680.06792(17)		2221f–0220f	5850.91092(17)	0.3999412(10)	1.372(13)	-4.04(43)	P50/R48	55/75	0.60	
4681.40342(9)	$\Pi-\Pi$	2111e–0110e	5266.71554(9)	0.39873802(22)	1.5167(13)	0.460(20)	P69/R65	109/120	0.38	
4681.4060(1)		2111e–0110e ^A		0.398738(1)	1.507(1)		P44/R38	/61	0.17	
4681.40361(11)		2111f–0110f	5266.71573(11)	0.39975328(26)	1.4201(15)	0.742(23)	P67/R67	114/123	0.47	
4681.4060(1)		2111f–0110f ^A		0.3997517(1)	1.3975(9)		P45/R37	/63	0.2	
4681.40403(49)		2111e–0110f	5266.71615(49)	0.3987341(35)	1.460(41)		Q29	15/23	0.93	
4681.40406(30)		2111f–0110e	5266.71618(30)	0.3997516(20)	1.405(23)		Q29	16/22	0.59	
4708.35262(41)	$\Pi-\Pi$	0910f–0110f	5293.66474(41)	0.4067406(26)	3.082(39)	-1.6(15)	P43/R41	51/61	1.14	
4708.35353(31)		0910e–0110e	5293.66565(31)	0.4039571(16)	2.856(21)	7.26(69)	P35/R45	50/59	0.88	
4751.97554(18)	$\Sigma-\Sigma$	3001e–0200e	5911.94725(18)	0.39724879(94)	1.200(12)	2.36(41)	P41/R44	65/70	0.55	3001e–0000e ^A
4845.88545(25)	$\Sigma-\Sigma$	4200e–0200e	6005.85716(25)	0.4032632(15)	4.704(21)	20.83(76)	P44/R42	70/81	0.85	
4848.10840(37)	$\Delta-\Delta$	4220e–0220e	6018.95140(37)	0.4036048(31)	-0.238(62)	-12.0(33)	P36/R35	47/58	0.96	
4848.10957(38)		4220f–0220f	6018.95257(38)	0.4036054(32)	2.356(66)	5.1(36)	P34/R34	48/57	0.90	
4856.43665(12)	$\Pi-\Pi$	0910f–0110f	5441.74877(12)	0.40434009(45)	2.4103(38)	0.332(86)	P55/R55	99/104	0.50	
4856.43695(9)		0910e–0110e	5441.74907(9)	0.40205224(37)	2.2714(33)	2.183(80)	P57/R52	98/104	0.39	
4865.47352(26)	$\Sigma-\Sigma$	5000e–1000e	6135.36550(26)	0.4009644(16)	2.920(22)	4.35(81)	P44/R42	66/75	0.89	
4867.3658(17)	$\Pi-\Sigma$	0312e–0200e	6027.3375(17)	0.3989307(82)	1.891(87)		P28/R27	17/22	1.27	
4867.36702(44)		0312f–0200e	6027.33873(44)	0.4002720(24)	2.088(24)		Q32	18/25	0.93	
4874.7365(41)	$\Phi-\Delta$	0332e–0220e	6045.5795(41)	0.400215(60)	11.4(27)	1.31E+03(36)	P20/R19	14/18	1.11	
4874.75571(52)		0332f–0220e	6045.59871(52)	0.3999573(33)	0.862(37)		Q30	15/19	0.96	
4892.60619(23)	$\Sigma-\Pi$	0202e–0110e	5477.91831(23)	0.3991320(12)	2.234(14)	2.57(44)	P47/R45	73/82	0.75	0202e–0000e ^A
4892.60663(24)		0202f–0110e	5477.91875(24)	0.39912770(74)	2.1657(39)		Q45	39/41	0.80	
4902.54207(30)	$\Delta-\Pi$	0222e–0110e	5487.85419(30)	0.3993702(15)	1.245(18)	-0.60(56)	P45/R46	69/74	0.95	
4902.54272(28)		0222e–0110f	5487.85484(28)	0.39937060(79)	1.2617(39)		Q49	36/43	0.86	
4902.54296(28)		0222f–0110f	5487.85508(28)	0.3993671(17)	1.671(23)	-0.28(85)	P44/R42	66/73	0.92	
4902.54349(32)		0222f–0110e	5487.85561(32)	0.39936560(80)	1.6679(37)		Q47	34/40	0.88	
4963.02359(18)	$\Sigma-\Sigma$	5000e–1000e	6232.91557(18)	0.39873076(84)	1.7604(93)	4.71(27)	P50/R46	75/81	0.64	
4975.39364(21)	$\Sigma-\Sigma$	5000e–0200e	6135.36535(21)	0.4009646(15)	2.926(24)	4.6(10)	P42/R36	63/70	0.77	
4981.22132(13)	$\Pi-\Pi$	4110f–0110f	5566.53344(13)	0.40215996(57)	1.8011(53)	1.10(13)	P53/R52	86/95	0.55	
4981.22139(18)		4110e–0110e	5566.53351(18)	0.4003572(12)	1.895(18)	10.49(71)	P43/R41	76/79	0.63	
4981.22409(59)		4110f–0110e	5566.53621(59)	0.402098(19)	-2.6(13)		Q11	7/9	0.48	
4986.32438(52)	$\Delta-\Delta$	4220f–0220f	6157.16738(52)	0.4019038(35)	1.954(56)	7.6(24)	P40/R38	47/58	1.23	
4986.3254(13)		4220f–0220e	6157.1684(13)	0.401817(94)	-15(12)		Q8	6/7	1.12	
4986.32608(50)		4220e–0220e	6157.16908(50)	0.4018760(33)	0.706(52)	-11.6(22)	P40/R38	49/60	1.19	
5045.12297(27)	$\Sigma-\Sigma$	3400e–1000e	6315.01495(27)	0.3994187(10)	0.2562(68)		P40/R38	55/64	0.92	
5072.94189(89)	$\Sigma-\Sigma$	5000e–0200e	6232.91360(89)	0.3987346(31)	1.713(22)		P37/R36	32/46	1.57	
5086.35971(16)	$\Pi-\Pi$	3310e–0110e	5671.67183(16)	0.39969951(65)	1.2416(64)	1.09(17)	P55/R52	82/103	0.57	
5086.36063(15)		3310f–0110f	5671.67275(15)	0.40136306(35)	0.8670(15)		P54/R54	85/102	0.70	
5086.3623(16)		3310e–0110f	5671.6745(16)	0.3996937(25)	1.27(69)		Q18	8/14	1.84	
5086.3649(56)		3310f–0110e	5671.6770(56)	0.40138(11)	4.0(44)		Q14	5/10	1.69	
5110.43022(38)	$\Delta-\Delta$	3420f–0220f	6281.27322(38)	0.4010880(14)	1.1492(96)		P33/R39	47/63	1.29	

Table 2 (continued)

ΔG_v^a (cm^{-1})	Type	Bands ^b	G_v (cm^{-1})	B_v (cm^{-1})	$D_v \times 10^7$ (cm^{-1})	$H_v \times 10^{12}$ (cm^{-1})	Observed lines	n/N^c	RMS $\times 10^3$	In Refs. ^d
5110.43111(36)		3420e–0220e	6281.27411(36)	0.4010962(14)	1.5801(91)		P29/R39	44/60	1.21	
5155.04314(49)	$\Sigma-\Sigma$	3400e–0200e	6315.01485(49)	0.3994196(30)	0.269(36)		P30/R28	39/54	1.32	
5442.02726(44)	$\Pi-\Pi$	0312e–0110f	6027.33938(44)	0.4002660(18)	2.009(14)		P39/R36	49/67	1.41	
5442.02763(48)		0312e–0110e	6027.33975(48)	0.3989271(19)	1.902(14)		P38/R36	47/63	1.26	
5526.04106(24)	$\Sigma-\Sigma$	2002e–1000e	6795.93304(24)	0.39501646(81)	1.4311(48)		P47/R44	70/81	1.00	
5542.38016(69)	$\Sigma-\Sigma$	1202e–0200e	6702.35187(69)	0.3974580(43)	2.260(52)		P34/R34	31/53	1.31	
5545.37509(41)	$\Delta-\Delta$	1222e–0220e	6716.21809(41)	0.3979379(23)	1.196(25)		P31/R37	42/58	1.17	
5567.09536(27)	$\Pi-\Pi$	1112f–0110f	6152.40748(27)	0.39765214(48)	1.5554(18)		P55/R56	58/109	0.71	
5567.0955(27)		1112f–0110e					Q5	0/5		
5567.09607(25)		1112e–0110e	6152.40819(25)	0.39682804(48)	1.5806(19)		P51/R50	59/99	0.68	
5683.56024(26)	$\Pi-\Pi$	2311f–0110f	6268.87236(26)	0.40280852(90)	2.4316(58)		P43/R39	63/80	0.92	
5683.56086(22)		2311e–0110e	6268.87298(22)	0.40072881(73)	2.2161(45)		P42/R40	69/80	0.85	
5795.63434(35)	$\Sigma-\Sigma$	4001e–1000e	7065.52632(35)	0.3971425(13)	2.0340(87)		P40/R40	62/75	1.28	
5797.92831(54)	$\Sigma-\Sigma$	3201e–0200e	6957.90002(54)	0.3996456(21)	3.001(16)		P37/R38	46/64	1.29	
5802.49936(57)	$\Delta-\Delta$	3221f–0220f	6973.34236(57)	0.4002510(41)	2.580(56)		P29/R27	33/45	1.38	
5802.50261(65)		3221e–0220e	6973.34561(65)	0.4001940(55)	0.429(85)		P25/R24	30/41	1.39	
5815.54236(13)	$\Pi-\Pi$	3111f–0110f	6400.85448(13)	0.40037293(31)	1.9138(14)		P54/R50	78/95	0.57	
5815.54274(14)		3111e–0110e	6400.85486(14)	0.39878693(30)	1.8425(11)		P53/R56	84/104	0.67	
5872.23809(36)	$\Sigma-\Sigma$	3201e–1000e	7142.13007(36)	0.3965276(19)	0.608(18)		P35/R34	49/62	1.06	
5905.55527(85)	$\Sigma-\Sigma$	4001e–0200e	7065.52698(85)	0.3971409(57)	2.043(73)		P27/R26	25/31	1.41	
5921.79904(15)	$\Pi-\Pi$	2311e–0110e	6507.11116(15)	0.39749601(69)	1.3473(74)	0.18(21)	P55/R51	77/102	0.52	
5921.79716(41)		3111e–0110e ^{f2}	6507.10928(41)	0.3974869(27)	1.145(40)	-8.9(16)	P17/R41	32/41	0.9	
5921.79929(17)		2311f–0110f	6507.11141(17)	0.39875735(39)	1.1200(17)		P54/R51	80/102	0.69	
5921.79520(44)		3111f–0110f ^{d2}	6507.10732(44)	0.3987653(23)	1.186(24)	1.45(68)	P16/R48	34/37	1.1	
5926.63654(71)	$\Delta-\Delta$	2421e–0220e	7097.47954(71)	0.3988480(51)	1.273(77)		P26/R24	26/34	0.98	
5988.3241(18)	$\Pi-\Pi$	4310f–0110f	6573.6362(18)	0.404989(20)	3.73(47)		P20/R20	14/22	1.71	
5988.3263(15)		4310e–0110e	6573.6384(15)	0.402011(11)	2.75(18)		P21/R22	17/27	1.25	
6124.3758(30)	$\Sigma-\Sigma$	6000e–1000e	7394.2678(30)	0.398899(17)	3.02(20)		P27/R26	16/24	1.43	
6127.31425(29)	$\Pi-\Pi$	5110f–0110f	6712.62637(29)	0.4026141(12)	2.3300(83)		P37/R38	60/71	1.07	
6127.31606(37)		5110e–0110e	6712.62818(37)	0.4001679(15)	2.139(12)		P35/R37	52/67	1.12	
6212.96512(50)	$\Sigma-\Sigma$	6000e–1000e	7482.85710(50)	0.3974331(26)	0.835(26)		P34/R29	38/52	1.36	
6244.63411(23)	$\Pi-\Pi$	5110e–0110e	6829.94623(23)	0.39876321(72)	1.4811(42)		P44/R49	61/86	0.82	
6244.63479(46)		5110e–0110e ^{f2}	6829.94850(46)	0.3987533(24)	1.382(24)		P31/R36	42/46	1.0	
6244.63508(27)		5110f–0110f	6829.94720(27)	0.4007641(16)	1.161(23)	-9.83(93)	P44/R42	63/80	0.79	
6244.63479(46)		5110f–0110f ^{d2}	6829.94691(49)	0.4007755(21)	1.377(17)		P31/R36	42/46	1.6	
6351.56220(32)	$\Pi-\Pi$	3510f–0110f	6936.87432(32)	0.4008533(15)	0.568(12)		P37/R34	58/67	1.21	
6351.56288(31)		3510e–0110e	6936.87500(31)	0.3987247(16)	0.956(16)		P36/R35	55/67	1.12	
6431.19910(75)	$\Delta-\Delta$	0223f–0220e	7602.04210(75)	0.396086(16)	1.00(59)		Q19	9/15	1.11	
6431.20040(25)		0223e–0220e	7602.04340(25)	0.39607088(95)	1.1468(66)		P45/R38	60/75	0.99	
6431.20114(45)		0223e–0220e ^{f2}	7602.04414(45)	0.3960717(18)	1.208(14)		P34/R36	33/37	1.0	
6432.51375(28)	$\Sigma-\Sigma$	0203e–0200e	7592.48546(28)	0.3958438(20)	2.267(32)	4.1(14)	P41/R40	62/76	0.91	
6432.51683(75)		0203e–0200e ^{f2}	7592.48854(75)	0.3958236(64)	1.994(99)		P26/R20	19/19	1.2	
6432.60805(92)	$\Sigma-\Sigma$	1003e–1000e	7702.50003(92)	0.3931132(44)	1.645(40)		P31/R33	25/41	1.71	
6473.4297(14)	$\Pi-\Pi$	0113f–0110e	7058.7418(14)	0.395950(60)	14.3(48)		Q11	6/10	1.07	
6473.43376(25)		0113e–0110e	7058.74588(25)	0.39506865(41)	1.6438(14)		P57/R50	44/106	0.64	
6473.43530(54)		0113e–0110e ^{f1}	7058.74742(54)	0.3950686(14)	1.6477(61)		P50/R43	67/71	2.2	
6473.4343(15)		0113e–0110f	7058.7464(15)	0.395086(53)	4.7(37)		Q11	8/10	1.31	
6473.43490(28)		0113f–0110f	7058.74702(28)	0.3957732(46)	1.6575(15)		P57/R55	42/103	0.67	
6473.43182(59)		0113f–0110f ^{d1}	7058.74394(59)	0.3957746(15)	1.6557(68)		P50/R43	57/65	2.3	
6670.38676(72)	$\Pi-\Pi$	2112e–0110e	7255.69888(72)	0.3972457(44)	2.042(52)		P28/R27	28/45	1.22	
6670.38685(70)		2112f–0110f	7255.69897(70)	0.3986707(35)	2.095(36)		P32/R30	32/52	1.35	
7056.43673(49)	$\Pi-\Pi$	4111e–0110e	7641.74885(49)	0.3971156(21)	1.762(17)		P40/R38	35/65	1.19	
7056.43827(43)		4111f–0110f	7641.75039(43)	0.3988486(19)	1.816(17)		P32/R33	39/58	1.00	
7667.8096(18)	$\Pi-\Pi$	1113f–0110f	8253.1217(18)	0.3942929(81)	1.548(78)		P37/R37	16/69	1.38	
7667.8111(22)		1113e–0110e	8253.1232(22)	0.3943851(14)	1.535(32)		P37/R37	15/71	1.36	

Note: The lower state constants and those appearing between square brackets were fixed at the values of Ref. [14]. The uncertainties are given in parentheses in the unit of the last quoted digit. In the case of previously analyzed bands, the corresponding spectroscopic parameters are given in italics for comparison: ^tToth [14], ^AAmiot [13], ^LI Liu et al. [16], ^{L2}Liu et al. [17].

^a Difference between the upper and lower vibrational term values.

^b Normal mode labeling according to the maximum value of the modulo of the expansion coefficients of an eigenfunction. In the cases when there are two candidates for the same labeling or the modulo of two principal expansion coefficients practically coincide, we give in parentheses the second variant of the labeling. Note that as a result of strong vibrational mixing, the normal mode labeling of some states differs from that given in the previous analysis.

^c n , number of transitions included in the fit; N , number of assigned rotational transitions.

^d Previous observations of the upper level through a different transition.

^e Perturbed bands.

3.2. Band-by-band rotational analysis

For the unperturbed bands, rotational analysis was performed using the standard expression of the ro-vibration energy levels:

$$F_v(J) = G_v + B_v J(J+1) - D_v J^2(J+1)^2 + H_v J^3(J+1)^3 \quad (1)$$

where G_v is the vibrational term value, B_v is the rotational constant, and D_v and H_v are the centrifugal distortion constants. The spectroscopic parameters for an upper state were fitted directly to the observed line positions of the respective bands, and in the case of hot bands involving the e and f rotational levels, the ee , ef , fe , and ff subbands were considered, respectively. The lower state rotational con-

stants were constrained to the values used in the literature [14]. The observed line positions together with the residuals, are given in the **Supplementary Material** of this paper. The spectroscopic parameters retrieved from the fitting of the line positions are listed in **Table 2**. The RMS deviations (*obs.-calc.*) are on the order of $1.0 \times 10^{-3} \text{ cm}^{-1}$ which is consistent with the experimental accuracy of the line positions. For the 30 bands that have been reported in Refs. [13,14,16,17], the present work extends to find higher *J* value transitions and allows a refinement of the spectroscopic constants. They are reviewed and included in **Table 2**. Since some upper vibrational states have been reported through other bands, the corresponding bands and references are also indicated in the last column of the same table for completeness. Note that in some cases, the same upper vibrational state can be determined by several different bands. For example, the bands 0202e–0000e, 0202e–0200e, and 0202e–1000e reach the same 0202e upper state at $5477.9174 \text{ cm}^{-1}$. In this case, the spectroscopic parameters of the 0202e state determined by the 0202e–0200e band with more observed lines and less RMS is preferable. Note that in some bands, since only a few lines were observed, it was difficult to fit the H_v parameters for those bands; as a result, the corresponding H_v values in **Table 2** are left blank. For the 3220e–0110e and 1112f–0110e bands, we could not determine any ro-vibrational parameters, except for their assignments.

4. Discussion

The agreement of the vibrational term values (G_v) determined from different measurements is one of the criterions to verify the experimental accuracy. **Fig. 4** shows the ΔG_v deviations of our work from that of three previous works (Amiot [13], Toth [14], Liu [16,17]), as a function of wavenumber. The FTIR spectra from these works were well calibrated with the 1–0 band of CO by Guelachvili [21] for the work of Amiot, and the $^{14}\text{N}_2^{16}\text{O}$ and water lines for the works of Toth and Song. Our results are consistent with those of Toth, within the experimental uncertainties ($1 \times 10^{-3} \text{ cm}^{-1}$). Meanwhile, the results of Amiot have a systematic deviation of $-2.5 \times 10^{-3} \text{ cm}^{-1}$ from the results of Toth and Song. The ΔG_v values of the work of Liu [16,17] recorded with CRDS randomly deviate from other FTIR results. **Fig. 5** gives the difference between the line positions of the $^{15}\text{N}^{14}\text{N}^{16}\text{O}$ assigned in the FTS_{Song} and CRDS spectrum between 5900 and 6850 cm^{-1} . The RMS is 0.0015 cm^{-1} around the experimental uncertainty. So the probable reason is that the set of transitions used for the line fitting

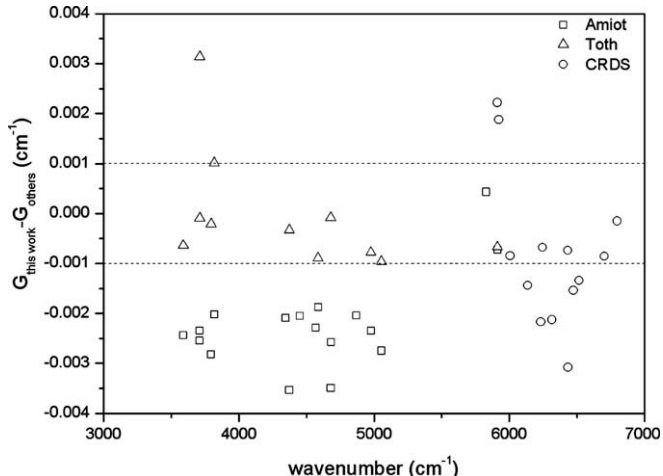


Fig. 4. Comparison of the difference of the upper and lower vibrational term values (G) given by Toth [14], Amiot [13], Liu [16,17] and this work.

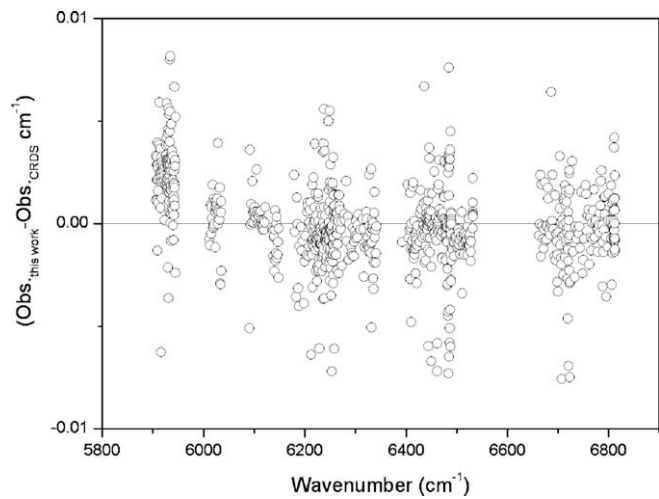


Fig. 5. Difference between the line positions of the $^{15}\text{N}^{14}\text{N}^{16}\text{O}$ assigned in FTS_{Song} spectrum and CRDS [16,17] spectrum between 5900 and 6850 cm^{-1} .

in CRDS include less transitions with low *J* values, then the G_v value is less accurate because low *J* values transitions are not in the input data file and the extrapolation of G_v at $J = 0$ is more uncertain.

In this work, some states were found to be affected by some interactions, which have not been included in the effective Hamiltonian model. As an example, **Fig. 6** shows the deviations of the calculated energy levels using the spectroscopic parameters in **Table 2** and the effective Hamiltonian models from the observed values of the 1201e state. It is clear that the perturbations of the ro-vibrational states happen near the two energy crossing points around $J = 39$ and $J = 60$.

Through the comprehensive comparisons of all the parameters listed in **Table 2**, some preferences are suggested: (1) the lower vibrational state of the band centered around 4317.01 cm^{-1} is the 0220e state, instead of the 0200e state given by Amiot (Ref. [13]). (2) the line positions of the *R* branch of the 0113–0110 $\Pi-\Pi$ hot band given with CRDS [16] are more accurate because the *R* branch of this band observed in present work was not resolved for the *e-e* and *f-f* sub-bands. For the same reason, the line positions of the *R* branch of the 1112–0110 and the 1113–0110 $\Pi-\Pi$ hot bands should also be adopted with caution.

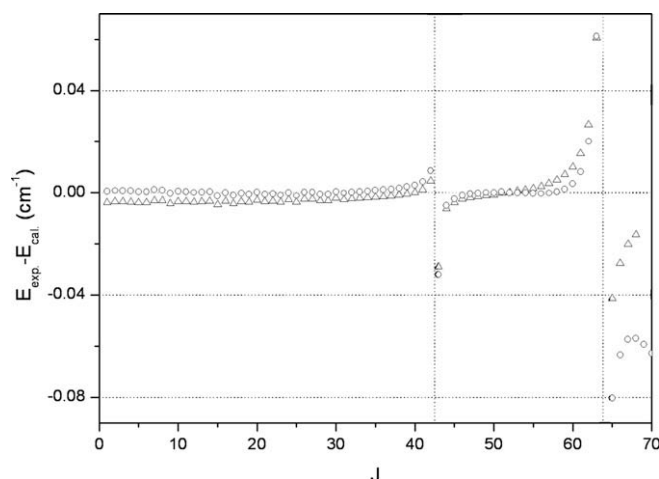


Fig. 6. The difference between the observed and calculated energy levels of the 1201e state of $^{15}\text{N}^{14}\text{N}^{16}\text{O}$. The open circles and triangles are according to the calculation using the spectroscopic parameters of **Table 2** and the effective Hamiltonian models, respectively.

Acknowledgments

Dr. F. Qi of NSRL is acknowledged for the PIMS mass spectrometry measurements. The authors thank Dr. V.I. Perevalov for providing the absorption spectrum calculations on the basis of global effective Hamiltonian models. This work is jointly supported by NSFC-China (Grant Nos. 20473079, 10574124 and 20873132), the Fok Ying Tong Education Foundation (101013), and the Chinese Ministry of Science and Technology (2007CB815203).

Appendix A. Supplementary data

Supplementary data for this article are available on ScienceDirect (www.sciencedirect.com) and as part of the Ohio State University Molecular Spectroscopy Archives (http://library.osu.edu/sites/msa/jmsa_hp.htm).

Supplementary data associated with this article can be found, in the online version, at doi:[10.1016/j.jms.2009.02.008](https://doi.org/10.1016/j.jms.2009.02.008).

References

- [1] F.K. Tittel, A.A. Kosterev, Appl. Phys. B 85 (2006) 171.
- [2] T. Röckmann, J. Kaiser, C.A.M. Brenninkmeijer, W.A. Brand, Rapid Commun. Mass Spectrom. 17 (2003) 1897–1908.
- [3] S.-M. Hu, O.N. Ulenikov, E.S. Bekhtereva, G.A. Onopenko, S.-G. He, H. Lin, J.-X. Cheng, Q.-S. Zhu, J. Mol. Spectrosc. 212 (2002) 89.
- [4] A.-W. Liu, O. Naumenko, K.-F. Song, B. Voronin, S.-M. Hu, J. Mol. Spectrosc. 236 (2006) 127.
- [5] A.-W. Liu, S.-M. Hu, C. Campy-Peyret, J.-Y. Mandin, O. Naumenko, B. Voronin, J. Mol. Spectrosc. 237 (2006) 53.
- [6] A.-W. Liu, J.-H. Du, K.-F. Song, L. Wang, L. Wan, S.-M. Hu, J. Mol. Spectrosc. 238 (2006) 11.
- [7] L. Wang, V.I. Perevalov, S.A. Tashkun, A.-W. Liu, S.-M. Liu, J. Mol. Spectrosc. 233 (2005) 297.
- [8] L. Wang, V.I. Perevalov, S.A. Tashkun, S.-M. Liu, J. Mol. Spectrosc. 234 (2005) 84.
- [9] L. Wang, V.I. Perevalov, S.A. Tashkun, K.-F. Song, S.-M. Hu, J. Mol. Spectrosc. 247 (2008) 64.
- [10] A.-W. Liu, O.N. Ulenikov, G.A. Onopenko, O.V. Gromova, E.S. Bekhtereva, L. Wan, L.-Y. Hao, S.-M. Hu, J.-M. Flaud, J. Mol. Spectrosc. 238 (2006) 11.
- [11] H.-Y. Ni, K.-F. Song, V.I. Perevalov, S.A. Tashkun, A.-W. Liu, L. Wang, S.-M. Hu, J. Mol. Spectrosc. 248 (2008) 41–60.
- [12] B. Drouin, F.W. Maiwald, J. Mol. Spectrosc. 236 (2006) 150.
- [13] C. Amiot, J. Mol. Spectrosc. 59 (1976) 191–208.
- [14] R. Toth, J. Mol. Spectrosc. 197 (1999) 158–187.
- [15] H. Herbin, N. Picque, G. Guelachvili, E. Sorokin, I. Sorokina, J. Mol. Spectrosc. 238 (2006) 256.
- [16] A.-W. Liu, S. Kassi, P. Malara, D. Romanini, V.I. Perevalov, S.A. Tashkun, S.-M. Hu, A. Campargue, J. Mol. Spectrosc. 244 (2007) 33–47.
- [17] A.-W. Liu, S. Kassi, V.I. Perevalov, S.A. Tashkun, A. Campargue, J. Mol. Spectrosc. 244 (2007) 48–62.
- [18] L.S. Rothman, D. Jacquemart, A. Barbe, D.C. Benner, M. Birk, L.R. Brown, M.R. Carleer, C. Chackerian Jr., K. Chance, V. Dana, V.M. Devi, J.-M. Flaud, R.R. Gamache, A. Goldman, J.-M. Hartmann, K.W. Jucks, A.G. Maki, J.Y. Mandin, S.T. Massie, J. Orphal, A. Perrin, C.P. Rinsland, M.A.H. Smith, J. Tennyson, R.N. Tolchenov, R.A. Toth, J. Vander Auwera, P. Varanasi, J. Quant. Spectrosc. Radiat. Transf. 96 (2005) 139–204.
- [19] J.-L. Teffo, V.I. Perevalov, O.M. Lyulin, J. Mol. Spectrosc. 168 (1994) 390–403.
- [20] A.V. Vlasova, B.V. Perevalov, S.A. Tashkun, V.I. Perevalov, in: Fifteenth Symposium on High Resolution Molecular Spectroscopy, Nizhnii Novgorod (Russia), 18–21 July 2006, Poster D20, pp. 86.
- [21] G. Guelachvili, in: Proceedings of A.M.C.O.V., Paris, Plenum Press, 1975.
- [22] R.A. Toth. Available from: <<http://mark4sun.jpl.nasa.gov/n2o.html>>.